Nat Microbiol. Author manuscript; available in PMC 2017 September 06.

Published in final edited form as:

Nat Microbiol. ; 2: 17028. doi:10.1038/nmicrobiol.2017.28.

Pentamidine sensitizes Gram-negative pathogens to antibiotics and overcomes acquired colistin resistance

Jonathan M. Stokes[1], **Craig R. MacNair**[1], **Bushra Ilyas**[1], **Shawn French**[1], **Jean-Philippe Côté**[1], **Catrien Bouwman**[2], **Maya A. Farha**[1], **Arthur O. Sieron**[1], **Chris Whitfield**[2], **Brian K. Coombes**[1], and **Eric D. Brown**[1,*]

[1]Michael G. DeGroote Institute for Infectious Disease Research, Department of Biochemistry and Biomedical Sciences, McMaster University, Hamilton, Ontario, Canada, L8N 3Z5

[2]Department of Molecular and Cellular Biology, University of Guelph, Guelph, Ontario, Canada, N1G 2W1

Abstract

The increasing use of polymyxins[1] in addition to the dissemination of plasmid-borne colistin resistance threatens to cause a serious breach in our last line of defense against multidrug resistant Gram-negative pathogens, and heralds the emergence of truly pan-resistant infections. Colistin resistance often arises through covalent modification of lipid A with cationic residues such as phosphoethanolamine (PEtN) – as is mediated by Mcr-1[2] – which reduce the affinity of polymyxins for lipopolysaccharide (LPS)[3]. Thus, new strategies are needed to address the rapidly diminishing number of treatment options for Gram-negative infections[4]. The difficulty in eradicating Gram-negative bacteria is largely due to a highly impermeable outer membrane, which serves as a barrier to many otherwise effective antibiotics[5]. Here, we describe an unconventional screening platform designed to enrich for non-lethal, outer membrane-active compounds with potential as adjuvants for conventional antibiotics. This approach identified the antiprotozoal drug pentamidine[6] as an effective perturbant of the Gram-negative outer membrane through its interaction with LPS. Pentamidine displayed synergy with antibiotics typically restricted to Gram-positive bacteria, yielding effective drug combinations with activity against a wide range of Gram-negative pathogens *in vitro*, and against systemic *Acinetobacter baumannii* infections in mice.

*Correspondence: ebrown@mcmaster.ca.

Author Contributions

J.M.S., C.R.M., B.I., S.F., J.P.C., C.B., C.W., B.K.C., and E.D.B. designed experiments; J.M.S. designed the vancomycin suppression screening platform; S.F., J.P.C., and J.M.S. performed genetic screens; J.M.S. performed the chemical screen; S.F. performed atomic force microscopy; C.B. performed core OS, LPS shedding, and periplasmic leaking assays with input from C.W. and J.M.S.; J.M.S. performed *in vitro* antibiotic susceptibility assays; B.I. performed qRT-PCR experiments; A.O.S. designed the pGDP2:*mcr-1* plasmid; J.M.S. engineered the *mcr-1* positive strains of *E. coli* BW25113 and *K. pneumoniae* ATCC 43816, and generated the colistin resistant variant of *A. baumannii* ATCC 17978; C.R.M., B.I., and B.K.C. designed *in vivo* infection model experiments; C.R.M., B.I., and J.M.S. performed *in vivo* infection model experiments; J.M.S., M.A.F., and E.D.B. wrote the manuscript with input from all authors.

Competing Financial Interests

The authors declare no competing financial interests.

Data availability: Large screening datasets can be found in Supplementary Data. The sequence of the pGDP2:*mcr-1* plasmid has been deposited to GenBank under accession number KX859085. Additional data that support the findings of this study are available from the corresponding author upon request.

Notably, the adjuvant activity of pentamidine persisted in polymyxin resistant bacteria *in vitro* and *in vivo*. Overall, pentamidine and structural analogs represent unexploited molecules for the treatment of Gram-negative infections, particularly those having acquired polymyxin resistance determinants.

Previous work by our group has shown that *E. coli* becomes susceptible to vancomycin during periods of cold stress[7]. Paradoxically, this phenotype could be reversed through inactivation of genes involved in outer membrane biosynthesis, particularly those required for core oligosaccharide (core OS) of LPS[8]. Given that genetic lesions in non-essential outer membrane biosynthesis often sensitize Gram-negative species to canonical Gram-positive antibiotics[9], we reasoned that screening for vancomycin antagonism at low temperature would yield non-lethal molecules that perturb the outer membrane. As a proof-of-principle, a comparative analysis of *E. coli* gene deletion mutants that resisted the action of vancomycin at 15°C, and those that showed enhanced sensitivity to the Gram-positive antibiotics erythromycin, novobiocin, and/or rifampicin at 37°C, revealed many common genes coding for functions in outer membrane biosynthesis (Fig. 1a and Supplementary Table 1). In agreement with this observation, an analysis of all gene deletion mutants displaying vancomycin resistance at 15°C revealed a significant enrichment for genes encoding functions in LPS and carbohydrate biosynthesis, as well those responsible for lipid metabolism and transport (Fig. 1b and Supplementary Table 2), all of which are essential to maintain outer membrane integrity. Together, these results show that screening for vancomycin antagonism at low temperature is capable of enriching for gene products necessary for outer membrane biosynthesis.

We subsequently leveraged these observations to develop a unique small molecule screening platform to detect non-lethal compounds that perturb outer membrane architecture. Indeed, molecules that preferentially target the outer membrane have long been sought after as antibiotic adjuvants[10], however none have successfully entered the clinic[11]. Importantly, the sensitivity and specificity of this cold-dependent phenotype in capturing an outer membrane-centric target list renders it a powerful platform for drug screening, as conventional antibiotic sensitization screens often capture large numbers of hit compounds with extraneous activities (Supplementary Table 1).

We therefore performed a screen of 1,440 previously approved drugs for those that suppressed the activity of vancomycin against *E. coli* at 15°C (Supplementary Table 3). Only 3 active compounds were identified, highlighting the specificity of this screening approach. We pursued these actives by assessing their ability to suppress vancomycin activity at 15°C in a dose-dependent manner against wild type *E. coli*, and subsequently counter screened for vancomycin suppression in *E. coli* expressing *mcr-1*. Pentamidine, used for the treatment of pneumocystis pneumonia and West African trypanosomiasis, displayed the most potent suppression of vancomycin activity against wild type *E. coli* (Fig. 1c and Supplementary Fig. 1), and was prioritized for further analysis. Interestingly, expression of *mcr-1* did not impair the ability of pentamidine to suppress vancomycin activity at low temperature (Fig. 1d).

Conseistent with an ability to suppress vancomycin activity, atomic force microscopy of pentamidine-treated *E. coli* revealed a dramatic effect on outer membrane structure at 37°C. Here, the surface topography of pentamidine-treated cells was characterized by undulations on the order of 40 nm in amplitude, whereas untreated *E. coli* remained largely uniform (Fig. 1e and Supplementary Fig. 2). Analysis of *E. coli* LPS upon treatment with pentamidine at 37°C failed to show inhibition of core OS biosynthesis (Supplementary Fig. 3a), suggesting that pentamidine may directly associate with the outer membrane. Consistently, pentamidine resulted in enhanced release of LPS from the outer membrane of *E. coli* (Supplementary Fig. 3a), similar to that previously observed with polymyxins[12] and other outer membrane stressors[13]. Additionally, pentamidine failed to cause the release of periplasmic or cytoplasmic proteins, as did polymyxin B nonapeptide (PMBN) and a sub-inhibitory concentration of polymyxin B (Supplementary Fig. 3b), in agreement with prior work[14,15]. Indeed, it has been shown that pentamidine displays high affinity for purified lipid A *in vitro* (K_d ~ 120 nM)16, consistent with the aforementioned observations.

Pentamidine has previously been reported to display a variety of activities depending on biological context. These include, for example, inhibition of both mitochondrial tRNA charging in *Saccharomyces cerevisiae*[17], and group I intron ribozymes in *Pneumocystis carinii* and *Candida albicans*[18]. Additionally, pentamidine has been shown to inhibit undecaprenyl diphosphate synthase (UppS) from *E. coli* and *Staphylococcus aureus in vitro*, and bind purified DNA with low affinity[19]. Nevertheless, the idiosyncratic antagonism by pentamidine of growth inhibition by vancomycin at 15°C, as well as the outer membrane perturbations upon pentamidine treatment at 37°C, strongly support a primary mechanism of action involving outer membrane disruption in the specific context of a Gram-negative bacterium. Further, we saw no enhanced activity of pentamidine (alone) against a strain of *E. coli* expressing a truncated LPS variant (Supplementary Fig. 4), a finding inconsistent with the hypothesis that this molecule functioned through inhibition of an intracellular target.

Given its ability to disrupt outer membrane architecture, we reasoned that pentamidine would act as an antibiotic adjuvant capable of sensitizing Gram-negative bacteria to antibiotics typically restricted to Gram-positive bacteria. Reminiscent of the ability of PMBN to potentiate large molecular weight antibiotics through electrostatic associations with lipid A[15], pentamidine potentiated the activity of Gram-positive antibiotics against *E. coli* at 37°C (Fig. 2a). Specifically, pentamidine synergized with rifampicin, novobiocin, and erythromycin (fractional inhibitory concentration [FIC] index ≤0.5; see Methods), all of which are hydrophobic, but not with the hydrophilic glycopeptide vancomycin. These data are consistent with antibiotic potentiation by PMBN, where synergy with hydrophobic molecules is generally more pronounced than that with hydrophilic molecules[20]. Additionally, pentamidine failed to significantly enhance the activity of low molecular weight antibiotics that can passively diffuse through the outer membrane, or gain access to the cytoplasm through membrane porins (Supplementary Fig. 5a).

To further investigate the ability of pentamidine to disrupt outer membrane integrity through association with LPS, we tested the effect of adding exogenous LPS into the growth medium. Addition of increasing concentrations of purified *E. coli* LPS to growth medium abolished pentamidine-dependent potentiation of rifampicin in a dose-dependent fashion

(Fig. 2b and Supplementary Fig. 5b). As expected, the presence of exogenous LPS also suppressed the ability of PMBN to potentiate rifampicin (Supplementary Fig. 5c). Interestingly, both pentamidine and PMBN failed to potentiate rifampicin when cells were grown in the presence of high concentrations of Mg^{2+} (Supplementary Fig. 5d), which promotes electrostatic interactions between adjacent LPS molecules[21]. These observations suggest that both adjuvants potentiate antibiotics through the disruption of lateral inter-LPS interactions. Consistent with this, pentamidine activated the PhoPQ two-component system, which is stimulated in Mg^{2+}-limiting conditions, and upon challenge with cationic peptides[3,22] (Fig. 2c and Supplementary Fig. 5e).

To gain further insight into the specific location where pentamidine associates with LPS, we analyzed the ability of pentamidine to potentiate rifampicin in *E. coli* mutants expressing truncated variants of core OS (Fig. 2d and Supplementary Fig. 5f). We observed that deeper truncations in core OS, or removal of core OS phosphate residues, resulted in more pronounced synergy, suggesting that pentamidine association with lipid A is a primary contributor to outer membrane disorganization. Indeed, a model whereby pentamidine disrupts lateral interactions between lipid A molecules was further supported through structure-function studies of pentamidine analogs. Specifically, we observed that both cationic amidine groups were essential for pentamidine activity (analogs 2 and 3), and that increasing the inter-amidine distance (analogs 4 and 8), increasing hydrophobicity (analogs 8 and 9), and decreasing molecular flexibility (analog 9) proportionately increased rifampicin potentiation against *E. coli* (Table 1).

To evaluate the spectrum of coverage by pentamidine against Gram-negative pathogens, we examined the *in vitro* activity of pentamidine in combination with rifampicin against a panel of clinical isolates. Pentamidine synergized with rifampicin against a wide phylogenetic distribution of antibiotic resistant strains, including naturally polymyxin resistant *Serratia* species (Fig. 2e and Supplementary Table 4). The lack of potentiation against *Pseudomonas aeruginosa* may be rationalized by the presence of additional phosphate residues in core OS[23], decreasing the access of pentamidine to lipid A. However, an explanation for the absence of potentiation in *Proteus* and *Morganella* species remains elusive. Indeed, all *Serratia*, *Proteus*, and *Morganella* isolates tested were highly resistant to polymyxin B (Supplementary Table 5).

The increasing clinical use of polymyxins to treat multidrug resistant Gram-negative infections[1], in combination with the global dissemination of plasmid-borne *mcr-1*, threatens the utility of these last line antibiotics. Indeed, we observed resistance to colistin – a clinically revived polymyxin – (Supplementary Fig. 6a) and to PMBN-dependent potentiation of rifampicin in *E. coli* expressing *mcr-1* (Fig. 3a). Notably, potentiation of rifampicin by pentamidine was retained upon expression of *mcr-1* (Fig. 3b and Supplementary Fig. 6b), suggesting that the action of pentamidine is independent of PEtN modifications on lipid A. Significantly, these phenotypes persisted in two environmental *E. coli* isolates harboring the *mcr-1* gene on natural plasmids (Fig. 3c, d and Supplementary Fig. 6c), and pentamidine retained adjuvant activity against *Klebsiella pneumoniae* expressing *mcr-1* (Supplementary Fig. 6d, e).

The broad *in vitro* efficacy of pentamidine in combination with antibiotics typically restricted to Gram-positive bacteria suggested there is strong potential to repurpose pentamidine for antibacterial use. Importantly, exposure of wild type *E. coli* to various combinations of pentamidine and rifampicin only generated mutants that displayed resistance to rifampicin (frequency of spontaneous resistance to rifampicin 4.2×10^{-8}; observed frequency of spontaneous resistance to pentamidine $< 8.3\times10^{-10}$; Supplementary Table 6), suggesting that pentamidine may maintain clinical efficacy without the rapid development of resistance. Interestingly, the whole-cell antibacterial activity of pentamidine has been recognized for upwards of 70 years in the context of both Gram-positive[19,24] and Gram-negative[19,25,26] bacteria, however this molecule has yet to be pursued as a modern clinical therapy, presumably due to insufficient potency *in vitro*. Indeed, with conventional knowledge suggesting that the concentrations of pentamidine required for activity *in vitro* are beyond those that are clinically achievable in humans, there have been no compelling data to suggest that pentamidine would display therapeutic efficacy *in vivo*. Furthermore, early clinical studies of pentamidine reported numerous side-effects, and only recently have advances been made to mitigate these risks[27].

Recognizing the potential of dose-sparing drug combinations in therapy[28], we tested the efficacy of pentamidine in combination with novobiocin in a systemic murine infection model of colistin sensitive *A. baumannii* (Fig. 4a), an opportunistic pathogen capable of acquiring horizontally-transferrable resistance determinants at high frequency[29], and increasingly displaying colistin resistance in the clinic[30]. While pentamidine synergized with rifampicin against clinical isolates of *A. baumannii* (Supplementary Table 4), pentamidine-dependent potentiation of novobiocin was considerably more potent, and as such this combination was selected for analysis of *in vivo* efficacy. Here, we observed 100% survival of mice treated with 10 mg/kg pentamidine in combination with 5 mg/kg novobiocin (Fig. 4b). These doses represent just $1/5^{th}$ and $1/20^{th}$ of human equivalent therapeutic doses, respectively, highlighting a remarkable dose-sparing effect. Furthermore, the majority of mice treated with this combination contained no detectable *A. baumannii* in organ tissue at day 7 post-infection (Fig. 4c and Supplementary Fig. 7a–d). Importantly, mice displayed organ occupancy of $\sim10^6$ CFU/ml/g at time of treatment (Supplementary Fig. 7e), showing that combination therapy cured an established infection.

We next tested the efficacy of this combination of pentamidine and novobiocin in a systemic murine infection model of colistin resistant *A. baumannii* (Fig. 4d and Supplementary Fig. 7f). In this pathogen, the principal mechanism underlying colistin resistance is PEtN modification of lipid A, similar to that imparted by Mcr-1, and involves mutations in *pmrAB*[22]. Consistently, our colistin resistant mutant displayed an A80V amino acid substitution in PmrA. Here, co-administration of 10 mg/kg pentamidine and 50 mg/kg novobiocin rescued 10 of 11 infected mice, and resulted in total clearance of bacteria in the spleen (Fig. 4e, f). Interestingly, previous work has shown that colistin resistant *A. baumannii* displays cross-resistance to host antimicrobial peptides[31]. Accordingly, our infection model may have required an elevated dose of novobiocin to aggressively halt infection given the diminished assistance of host innate immune factors.

The increasing incidence of spontaneous colistin resistance, as well as the acquisition of *mcr-1* by alarmingly common pathogens such as carbapenem resistant Enterobacteriaceae[32], is resulting in the emergence of untreatable infections and threatens to overwhelm healthcare practices worldwide. Here, we highlight the utility of a powerful screening platform, and introduce a use for the antiprotozoal drug pentamidine as an antibiotic adjuvant for the treatment of polymyxin resistant infections at subclinical doses *in vivo*. We posit that pentamidine and analogs thereof represent attractive leads as adjuvants to address the emerging threat of pan-resistant Gram-negative infections.

Methods

Genetic screening

The *E. coli* Keio collection[33] was pinned from frozen stocks at 1536-density onto solid LB media using a Singer RoToR automated pinning system (Singer Instruments). Media was supplemented with 64 μg/ml erythromycin, 128 μg/ml novobiocin, 8 μg/ml rifampicin, or 32 μg/ml vancomycin. All antibiotics were purchased from Sigma-Aldrich. Cells were grown at 37°C for 18 hours on LB containing erythromycin, novobiocin, or rifampicin, in duplicate. For low-temperature experiments, cells were grown at 15°C for 72 hours on LB containing vancomycin, in duplicate. After incubation, plates were scanned in transmissive mode on an Epson Perfection V750-M scanner (Epson) and quantitatively analyzed using ImageJ. Plate images were background subtracted using a 50-pixel rolling ball radius and converted to a binary image using the Otsu algorithm to identify colony margins. With colony margins identified, the integrated density (light absorption) of each was calculated as an indicator of cell number. Edge effects were corrected using a double-pass method across columns and rows based on the median value[34,35]. Strains grown at 37°C in the presence of erythromycin, novobiocin, or rifampicin with growth at least 3σ less than the mean were defined as sensitive. Strains grown at 15°C in the presence of vancomycin with growth at least 3σ greater than the mean were defined as resistant. Genetic intersections between the various treatments were identified with the R statistical programming language[36], and used to generate a 4-treatment Venn diagram. From the vancomycin resistant genetic subset of 41 strains, gene ontology (GO) terms were generated using EcoCyc pathway-tools[37–39]. This list was further refined to include transcriptional regulation and biosynthetic pathways using an enrichment analysis in EcoCyc pathway-tools. Counts of the number of genes present for each GO, biosynthetic pathway, or promoter activation classification were compiled, along with p-values, to assess statistical enrichment of cellular processes. ImageJ analyses for genetic screens were conducted using a recorded ImageJ macro. The Venn diagram generated using the R statistical programming language was calculated using the “intersect” function.

Chemical screening

E. coli BW25113 was grown overnight in LB media and diluted 1/5000 into fresh LB containing 16 μg/ml vancomycin. 49.5 μl of cells was subsequently transferred to each well of a clear 384-well flat-bottom plate (Corning) using a Beckman Coulter Biomek FX^P laboratory automated workstation (Beckman Coulter). 0.5 μl of each molecule from a library of 1440 previously approved drugs was added to cells using a 96-head pin tool (V&P

Scientific), in duplicate, such that the final screening concentration of each compound was 10 μM. Plates were immediately read at 600 nm using a Perkin Elmer EnVision plate reader (Perkin Elmer), then grown without shaking at 15°C for 96 hours. Plates were again read at 600 nm, and cell growth was calculated by subtracting the initial optical density (OD) of each well at time 0 from the final OD at 96 hours.

Checkerboard analyses

E. coli BW25113 was grown overnight in LB media and diluted 1/5000 into fresh LB. Vancomycin antagonism was determined by conducting standard checkerboard broth microdilution assays with 8 two-fold serially diluted concentrations of pentamidine (Sigma-Aldrich) and vancomycin against cells in a final volume of 100 μl. Plates were incubated without shaking at 15°C for 96 hours prior to reading at 600 nm. This duration was sufficient for untreated cultures to reach early-stationary phase. Antibiotic synergy was determined by diluting overnight cultures 1/10,000 into fresh LB and conducting checkerboard broth microdilution assays with 8 two-fold serially diluted concentrations of various antibiotics in final volumes of 100 μl. Plates were incubated at 37°C with continuous shaking in a Tecan Sunrise plate reader (Tecan), with reads at 600 nm taken every 10 minutes to monitor growth. At early-stationary phase for each strain, experiments were halted and final reads were used to generate checkerboard plots. All checkerboard experiments were conducted in at least 2 biological replicates; representative plots are shown throughout. For polymyxin resistant strains, overnights were grown in the presence of 50 μg/ml kanamycin (for *E. coli* BW25113 and *K. pneumoniae* ATCC 43816 transformed with pGDP2:*mcr-1*), or 2 μg/ml colistin (for *E. coli* strains carrying *mcr*-1 on natural plasmids and the spontaneous colistin resistant variant of *A. baumannii* ATCC 17978). The sequence of the pGDP2:*mcr-1* plasmid has been deposited to GenBank under accession number KX859085. Core OS mutants used to analyze pentamidine-dependent rifampicin potentiation were gathered from the *E. coli* Keio collection, except for the Δ*waaC* strain, which was engineered in wild type *E. coli* BW25113 using standard *E. coli* gene deletion techniques. Clinical isolates were curated from the Wright Clinical Collection. Isolation of the spontaneous colistin resistant *A. baumannii* variant was conducted by plating the colistin sensitive *A. baumannii* ATCC 17978 parent strain on 4 μg/ml colistin at 37°C for 48 hours, and subsequent purification of a single colony. Whole genome sequencing on an Illumina HiSeq platform revealed a point mutation in the *pmrA* gene, resulting in an A80V amino acid substitution in the N-terminal receiver domain. Pentamidine analogs were purchased from WuXi AppTech (Shanghai, China). LPS purified from *E. coli* 0127:B8 (Sigma-Aldrich) or $MgCl_2$ (Sigma-Aldrich) was used in synergy inhibition experiments. Fractional inhibitory concentration (FIC) indices[40] were calculated as described below: *MICa* is the minimum inhibitory concentration (MIC) of compound A alone; *MICac* is the MIC of compound A in combination with compound B; *MICb* is the MIC of compound B alone; *MICbc* is the MIC of compound B in combination with compound A; FICa is the FIC of compound A; FICb is the FIC of compound B. Synergy is defined as FIC index ≤0.5. Antagonism is defined as FIC index ≥4.

$$FICi = \frac{MICac}{MICa} + \frac{MICbc}{MICb} = FICa + FICb$$

Antibiotic potency analyses

Cells were grown overnight in LB media, with or without selection as described above, and diluted 1/10,000 into fresh LB. Cells were then introduced to 2-fold serial dilutions of antibiotic in a final volume of 100 µl. Plates were incubated at 37°C with continuous shaking in a Tecan Sunrise plate reader (Tecan), with reads at 600 nm taken every 10 minutes to monitor growth. At early-stationary phase for each strain, experiments were halted and final reads were used to generate antibiotic potency plots. A conservative clinical MIC breakpoint for colistin of 2 µg/ml was set by the Société Française de Microbiologie[41], and used to outline resistance in this study.

AFM sample preparation and imaging

Antibiotic treatments were prepared against *E. coli* BW25113 as described for antibiotic potency experiments. 50 µl of mid-log culture (OD~0.5) was transferred to hydrophilic polycarbonate 0.2 µm Millipore Isopore GTTP filters (Merck Millipore), on top of Kimwipes (Kimberly-Clark Professional) to absorb excess liquid across the filter. 50 µl of 25 mM HEPES pH 7.0 was then passed over the culture and absorbed by a Kimwipe in order to flush extracellular salts from the LB medium. Once the liquid had been removed, the filter was quickly attached to a clean glass slide with a non-conductive double-sided adhesive tab. Samples were imaged using a Bruker BioScope Catalyst (Bruker), with a Nanoscope V controller. For each treatment, a 0.65 µm thick Si_3N_4 triangular cantilever was used (Scan Asyst AIR, Bruker), with a symmetric tip and spring constant of ~0.4 $N{\cdot}m^{-1}$. Scans were acquired at 25°C, with scan rates of 0.5 Hz and 512 samples per line resolution, in PeakForce quantitative nanomechanical mapping mode. Downstream image processing and analysis was performed using NanoScope software (Bruker). Height images were flattened to compensate for cell curvature, and topographical sections were used to generate 2-dimensional and 3-dimensional reconstructions of surface texture. Representative scans of cells acquired from at least 2 independent experiments are shown.

Outer membrane analyses

20 ml cultures of *E. coli* BW25113 were grown at 37°C in LB containing various antibiotics until mid-log phase (OD~0.5). All experiments were performed in biological duplicate, and representative data are shown. For cell surface LPS analysis, the equivalent of 1 ml of cells at OD=1.0 were boiled in SDS-PAGE loading buffer for 10 minutes, and subsequently treated with proteinase K at 55°C for 3 hours. The LPS core OS bands were then resolved on NuPAGE Novex 4–12% Bis-Tris gradient gels (Life Technologies), and visualized by silver staining. For LPS shedding, the remainder of each culture was centrifuged at 5000xg for 15 minutes at 4°C, and 10 ml of each supernatant was dialyzed against water at 4°C for 24 hours in dialysis tubing (Spectra/Por MWCO 3.5 kDa). The dialyzed supernatants were then lyophilized, resuspended in 200 µl water ($1/50^{th}$ of original volume), and then normalized according to culture OD at harvest. Samples were boiled in SDS-PAGE loading buffer for 10

minutes, and subsequently treated with proteinase K at 55°C for 3 hours. The LPS core OS bands were then resolved on NuPAGE Novex 4–12% Bis-Tris gradient gels, and visualized by silver staining. For membrane leakage analyses, concentrated supernatant samples were resolved on 12% SDS-PAGE gels and transferred into nitrocellulose membranes. After blocking in 5% skim milk in TTBS for 2 hours, membranes were incubated with anti-maltose binding protein antibody (New England Biolabs) diluted 1/10,000 or anti-RNA polymerase alpha subunit antibody (BioLegend; 1/3000 dilution) overnight at 4°C. Membranes were washed in TTBS, and incubated with alkaline phosphatase-conjugated anti-mouse antibody (1/3000) in 3% BSA in TTBS for 2 hours. Membranes were again washed in TTBS and visualized with BCIP/NBT. For periplasmic shock treatment, *E. coli* BW25113 was grown at 37°C in LB to OD~1.0, and cells were harvested by centrifugation at 5000xg for 15 minutes at 4°C. Cells were resuspended in 3.5 ml buffer containing 100 mM Tris-HCl pH 8.0 + 500 mM sucrose, and incubated on ice for 5 minutes. Lysozyme was added to 100 μg/ml + 1mM EDTA pH 8.0, and incubated on ice for 20 minutes. $MgSO_4$ was added to a final concentration of 20 mM, and the periplasmic fraction was harvested by centrifugation at 12,000xg for 10 minutes at 4°C.

Quantitative reverse transcription PCR

Wild type *E. coli* BW25113 and *E. coli* BW25113 Δ*phoP* were grown overnight in LB media and diluted 1/5000 into 10 ml fresh LB supplemented with antibiotics as described. Cells were grown to mid-log phase (OD~0.5) at 37°C and pelleted by centrifugation. Cells were then lysed in 2 ml TRIzol (Life Technologies) and incubated at room temperature for 5 minutes, or frozen at −20°C for later processing. Phase separation was performed by phenol-chloroform extraction. 200 μl chloroform (Biobasic) was vigorously mixed with 1 ml TRIzol, followed by centrifugation at 12,000xg for 15 minutes at 4°C. The aqueous phase was collected, and RNA was isolated by isopropanol-ethanol extraction. The aqueous phase was mixed with 500 μl of 100% isopropanol (Biobasic) per 1 ml of TRIzol reagent. After incubation at room temperature for 10 minutes, RNA was pelleted by centrifugation at 12,000xg for 15 minutes at 4°C. RNA was then washed with 75% ethanol and centrifuged once more under the same conditions. The resulting pellet was allowed to air dry for 10 minutes to remove any remaining ethanol, and resuspended in 100 μl of RNase free water (Ambion). RNA was subject to DNase I treatment (Ambion) for 30 minutes at 37°C, followed by DNase inactivation. The RNA was then re-purified from DNase I by a subsequent isopropanol-ethanol wash step. RNA was mixed with isopropanol at −20°C for 30 minutes, pelleted by centrifugation, washed once with 75% ethanol, re-pelleted, and resuspended in water. Prior to cDNA synthesis, RNA from all isolates was adjusted to identical concentrations. 600 ng total RNA from each sample was used for reverse transcription using the Quanta Biosciences qScript cDNA supermix (Quanta Biosciences), as well as for a no RT control. First strand cDNA was diluted 1/10 prior to qRT-PCR, which was conducted in 96-well format using the Light cycler 480 (Roche) with SYBR Green (PerfeCTa SYBR green supermix, Quanta Biosciences). Primers JS02F and JS02R were used to amplify *mgtA*, which is upregulated in response to PhoPQ activation[42], and JS03F and JS03R were used to amplify the housekeeping gene *rsmC*. Cycle threshold values were used to calculate RNA concentrations based on a standard curve for each primer pair. RNA concentrations for *mgtA* were then normalized to the RNA concentrations of *rsmC*.

Experiments were conducted in technical and biological duplicates. JS02F – 5′cggtggtagtggcagaaaat3′; JS02R – 5′gtctcttttggcggatcaag3′; JS03F – 5′gaaattctggggcgaataca3′; JS03R –5′ctttcacctcggaaaagacg3′.

Pentamidine frequency of resistance analysis

E. coli BW25113 was grown overnight in LB media and concentrated to ~1×10^9 CFU/ml in fresh LB. 100 μl of cells was then transferred onto solid LB in 100 mm petri dishes (Fisher Scientific) supplemented with pentamidine and rifampicin as described. The final number of cells deposited onto each plate was 1.1×10^8 CFU/ml, as determined by serial plating onto non-selective LB. Cells were incubated at 37°C for 24 hours, and single colonies from each condition were isolated and re-streaked onto fresh LB plates containing the pentamidine/rifampicin combination from which each suppressor emerged. After a subsequent incubation at 37°C for 24 hours, reconfirming suppressors were grown in LB media overnight, and tested for rifampicin sensitivity as described for antibiotic potency experiments. After observing that all 61 reconfirming suppressor mutants displayed resistance to rifampicin, a representative selection of isolates was then tested for possible cross-resistance to pentamidine using checkerboard analyses at 37°C with pentamidine and novobiocin. All strains maintained pentamidine sensitivity. The observed frequency of resistance to pentamidine was then calculated as described below, based on the total number of pentamidine/rifampicin combinations (11 conditions; 1.1×10^8 CFU/condition) that displayed growth inhibition of *E. coli*. Using this calculation (61 suppressors; 13 conditions; 1.1×10^8 CFU/condition), the frequency of resistance to rifampicin was calculated at 4.2×10^{-8}, consistent with previous investigations[43,44].

$$\frac{<1}{11\times1.1\times10^8}<8.3\times10^{-10}$$

Mouse infection models

Animal experiments were conducted according to guidelines set by the Canadian Council on Animal Care using protocols approved by the Animal Review Ethics Board at McMaster University under Animal Use Protocol #13-07-20. Sample size was selected based on the results of a preliminary infection trial (n=3). Prior to infection, mice were relocated at random from a housing cage to treatment or control cages. No animals were excluded from analyses, and blinding was considered unnecessary. Seven to nine week old female C57BL/6 mice (Taconic Biosciences) were infected intraperitoneally with ~2×10^6 CFU colistin sensitive *A. baumannii* ATCC 17978, or the spontaneous colistin resistant variant of *A. baumannii* ATCC 17978, with 5% porcine mucin (Sigma-Aldrich). Infections were allowed to establish for 2 hours, and treatments were administered intraperitoneally as described. Clinical endpoint was determined using a 5-point body condition score analyzing weight loss, decrease in body temperature, respiratory distress, hampered mobility, and hunched posture. Experimental endpoint was defined as 7-days post-infection for mice not reaching clinical endpoint. Mice were euthanized and tissues were harvested into ice cold PBS at necropsy. Blood was collected into sterile 2 ml heparinized tubes (BD Scientific). Organs were homogenized using a high-throughput tissue homogenizer (Retsch), serially diluted in

PBS, and plated onto solid LB supplemented with 20 μg/ml chloramphenicol. Plates were incubated overnight at 37°C and colonies were quantified to determine organ load.

Supplementary Material

Refer to Web version on PubMed Central for supplementary material.

Acknowledgments

We thank Kali Iyer and Lindsey Carfrae for assistance with mouse infection experiments, and Dr. Michael Mulvey from the University of Manitoba for providing the environmental *mcr-1* positive *E. coli* isolates. This work was supported by Discovery and Foundation grants, respectively, from the Natural Sciences and Engineering Research Council, and Canadian Institutes of Health Research (FDN-143215), to E.D.B.; by grants from Cystic Fibrosis Canada and the Ontario Research Fund to E.D.B.; by a grant from the Michael G. DeGroote Institute for Infectious Disease Research to E.D.B. and B.K.C.; by an operating grant from the Canadian Institutes of Health Research to B.K.C. (MOP-82704); by a Foundation grant from the Canadian Institutes of Health Research to C.W. (FDN-CEHA-26119); by salary awards to E.D.B., B.K.C., and C.W. from the Canada Research Chairs Program; by a fellowship from the Fonds de reserche en santé du Québec to J.P.C.; by a fellowship from the Canadian Institutes of Health Research DSECT Program to S.F.; by a scholarship from the Ontario Graduate Scholarships Program to C.R.M.; and by scholarships to J.M.S. from the Canadian Institutes of Health Research and the Ontario Graduate Scholarships Program.

References

1. Nation RL, Li J. Colistin in the 21st century. Curr Opin Infect Dis. 2009; 22:535–543. [PubMed: 19797945]
2. Liu YY, et al. Emergence of plasmid-mediated colistin resistance mechanism MCR-1 in animals and human beings in China: a microbiological and molecular biological study. Lancet Infect Dis. 2016; 16:161–168. [PubMed: 26603172]
3. Needham BD, Trent MS. Fortifying the barrier: the impact of lipid A remodelling on bacterial pathogenesis. Nat Rev Microbiol. 2013; 11:467–481. [PubMed: 23748343]
4. Brown ED, Wright GD. Antibacterial drug discovery in the resistance era. Nature. 2016; 529:336–343. [PubMed: 26791724]
5. Nikaido H. Molecular basis of bacterial outer membrane permeability revisited. Microbiol Mol Biol Rev. 2003; 67:593–656. [PubMed: 14665678]
6. Sands M, Kron MA, Brown RB. Pentamidine: a review. Rev Infect Dis. 1985; 7:625–634. [PubMed: 3903942]
7. Stokes JM, Davis JH, Mangat CS, Williamson JR, Brown ED. Discovery of a small molecule that inhibits bacterial ribosome biogenesis. Elife. 2014; 3:e03574. [PubMed: 25233066]
8. Stokes JM, et al. Cold stress makes *Escherichia coli* susceptible to glycopeptide antibiotics by altering outer membrane integrity. Cell Chem Biol. 2016; 23:267–277. [PubMed: 26853624]
9. Delcour AH. Outer membrane permeability and antibiotic resistance. Biochim Biophys Acta. 2009; 1794:808–816. [PubMed: 19100346]
10. Nikaido H. Prevention of drug access to bacterial targets: permeability barriers and active efflux. Science. 1994; 264:382–388. [PubMed: 8153625]
11. Gill EE, Franco OL, Hancock RE. Antibiotic adjuvants: diverse strategies for controlling drug-resistant pathogens. Chem Biol Drug Des. 2015; 85:56–78. [PubMed: 25393203]
12. Band VI, Weiss DS. Mechanisms of antimicrobial peptide resistance in Gram-negative bacteria. Antibiotics. 2015; 4:18–41. [PubMed: 25927010]
13. MacDonald IA, Kuehn MJ. Offense and defense: microbial membrane vesicles play both ways. Res Microbiol. 2012; 163:607–618. [PubMed: 23123555]
14. Vaara M. Agents that increase the permeability of the outer membrane. Microbiol Rev. 1992; 56:395–411. [PubMed: 1406489]
15. Vaara M, Vaara T. Polycations as outer membrane-disorganizing agents. Antimicrob Agents Chemother. 1983; 24:114–122. [PubMed: 6194743]

16. David SA. Towards a rational development of anti-endotoxin agents: novel approaches to sequestration of bacterial endotoxins with small molecules. J Mol Recognit. 2001; 14:370–387. [PubMed: 11757070]
17. Sun T, Zhang Y. Pentamidine binds to tRNA through non-specific hydrophobic interactions and inhibits aminoacylation and translation. Nucleic Acids Res. 2008; 36:1654–1664. [PubMed: 18263620]
18. Miletti KE, Leibowitz MJ. Pentamidine inhibition of group I intron splicing in *Candida albicans* correlates with growth inhibition. Antimicrob Agents Chemother. 2000; 44:958–966. [PubMed: 10722497]
19. Zhu W, et al. Antibacterial drug leads: DNA and enzyme multitargeting. J Med Chem. 2015; 58:1215–1227. [PubMed: 25574764]
20. Ofek I, et al. Antibacterial synergism of polymyxin B nonapeptide and hydrophobic antibiotics in experimental gram-negative infections in mice. Antimicrob Agents Chemother. 1994; 38:374–377. [PubMed: 8192470]
21. Clifton LA, et al. Effect of divalent cation removal on the structure of Gram-negative bacterial outer membrane models. Langmuir. 2014; 31:404–412. [PubMed: 25489959]
22. Olaitan AO, Morand S, Rolain JM. Mechanisms of polymyxin resistance: acquired and intrinsic resistance in bacteria. Front Microbiol. 2014; 5:643. [PubMed: 25505462]
23. Bystrova OV, et al. Structural studies on the core and the O-polysaccharide repeating unit of *Pseudomonas aeruginosa* immunotype 1 lipopolysaccharide. Eur J Biochem. 2002; 269:2194–2203. [PubMed: 11985598]
24. Schoenbach EB, Greenspan EM. The pharmacology, mode of action and therapeutic potentialities of stilbamidine, pentamidine, propamidine and other aromatic diamidines a review. Medicine (Baltimore). 1948; 27:327–377. [PubMed: 18885033]
25. Amos H, Vollmayer E. Effect of pentamidine on the growth of *Escherichia coli*. J Bacteriol. 1957; 73:172–177. [PubMed: 13416166]
26. Ando M, et al. In situ potentiometric method to evaluate bacterial outer membrane-permeabilizing ability of drugs: example using antiprotozoal diamidines. J Microbiol Methods. 2012; 91:497–500. [PubMed: 23046554]
27. Yeung KT, Chan M, Chan CK. The safety of i. v pentamidine administered in an ambulatory setting. Chest. 1996; 110:136–140. [PubMed: 8681617]
28. Ejim L, et al. Combinations of antibiotics and nonantibiotic drugs enhance antimicrobial efficacy. Nat Chem Biol. 2011; 7:348–350. [PubMed: 21516114]
29. Dijkshoorn L, Nemec A, Seifert H. An increasing threat in hospitals: multidrug-resistant *Acinetobacter baumannii*. Nat Rev Microbiol. 2007; 5:939–951. [PubMed: 18007677]
30. Qureshi ZA, et al. Colistin-resistant *Acinetobacter baumannii*: beyond carbapenem resistance. Clin Infect Dis. 2015; 60:1295–1303. [PubMed: 25632010]
31. Napier BA, et al. Clinical use of colistin induces cross-resistance to host antimicrobials in *Acinetobacter baumannii*. mBio. 2013; 4:e00021–13. [PubMed: 23695834]
32. Du H, Chen L, Tang YW, Kreiswirth BN. Emergence of the mcr-1 colistin resistance gene in carbapenem-resistant Enterobacteriaceae. Lancet Infect Dis. 2016; 16:287–288. [PubMed: 26842776]
33. Baba T, et al. Construction of *Escherichia coli* K-12 in-frame, single-gene knockout mutants: the Keio collection. Mol Syst Biol. 2006; 2 2006.0008.
34. Mangat CS, Bharat A, Gehrke SS, Brown ED. Rank ordering plate data facilitates data visualization and normalization in high-throughput screening. J Biomol Screen. 2014; 19:1314–1320. [PubMed: 24828052]
35. French S, et al. A robust platform for chemical genomics in bacterial systems. Mol Biol Cell. 2016; 27:1015–1025. [PubMed: 26792836]
36. Ihaka R, Gentleman R. R: a language for data analysis and graphics. J Comp Graph Stat. 1996; 5:299–314.
37. Keseler IM, et al. EcoCyc: fusing model organism databases with systems biology. Nucleic Acids Res. 2013; 41:D605–D612. [PubMed: 23143106]

38. Karp PD. Pathway databases: a case study in computational symbolic theories. Science. 2001; 293:2040–2044. [PubMed: 11557880]

39. Karp PD, et al. Pathway Tools version 19.0 update: software for pathway/genome informatics and systems biology. Brief Bioinform. 2016; 17:877–890. [PubMed: 26454094]

40. Odds FC. Synergy, antagonism, and what the chequerboard puts between them. J Antimicrob Chemother. 2003; 52:1. [PubMed: 12805255]

41. Hasman H, et al. Detection of mcr-1 encoding plasmid-mediated colistin-resistant *Escherichia coli* isolates from human bloodstream infection and imported chicken meat, Denmark 2015. Euro Surveill. 2015; 20

42. Groisman EA. The pleiotropic two-component regulatory system PhoP-PhoQ. J Bacteriol. 2001; 183:1835–1842. [PubMed: 11222580]

43. O'Neill AJ, Cove JH, Chopra I. Mutation frequencies for resistance to fusidic acid and rifampicin in *Staphylococcus aureus*. J Antimicrob Chemother. 2001; 47:647–650. [PubMed: 11328777]

44. Mariam DH, Mengistu Y, Hoffner SE, Andersson DI. Effect of rpoB mutations conferring rifampin resistance on fitness of *Mycobacterium tuberculosis*. Antimicrob Agents Chemother. 2004; 48:1289–1294. [PubMed: 15047531]

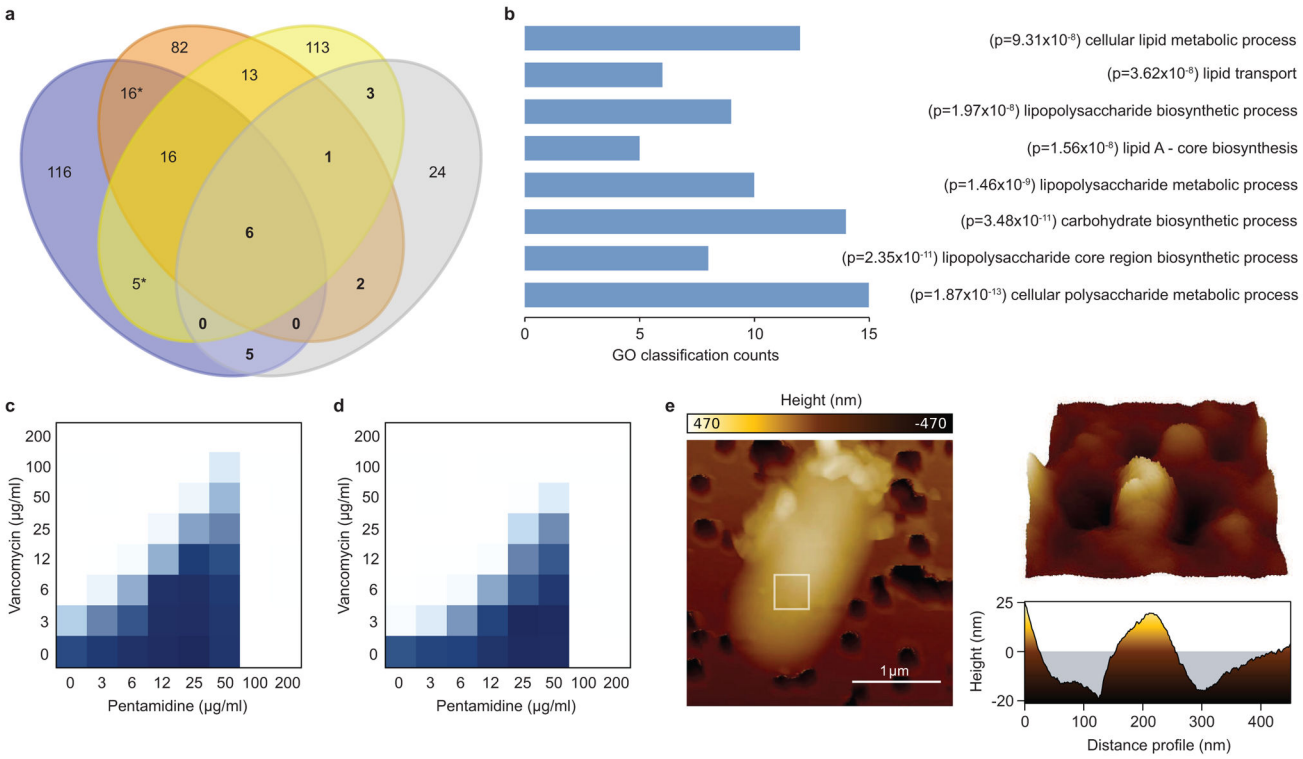

Figure 1. A vancomycin antagonism screening platform identifies pentamidine

a, Venn diagram showing the number of gene deletion mutants that displayed sensitivity to novobiocin (blue), rifampicin (orange), and/or erythromycin (yellow) at 37°C, and/or resistance to vancomycin (grey) at 15°C. The *E. coli* gene deletion (Keio) collection was arrayed on solid LB media containing sub-inhibitory concentrations of each antibiotic, and sensitivity or resistance was determined by analyzing colony growth[35]. Bold numbers highlight the genes that displayed sensitivity to any combination of novobiocin, rifampicin, or erythromycin, as well as resistance to vancomycin. **b,** 41 gene deletion mutants that displayed resistance to vancomycin at 15°C were classified based on gene ontology (GO), biosynthetic pathway, or promoter activation, and statistical enrichment was calculated using EcoCyc pathway-tools[37–39]. Enrichment was based on functional overrepresentation of the genes resulting in vancomycin resistance, using a Fisher's exact test to calculate p-value. Calculations were performed in pathway-tools using the enrichment analysis function without multiple hypothesis correction. The 8 most statistically enriched, non-redundant GO, biosynthetic pathway, and promoter activation classifications are shown. **c,** Checkerboard broth microdilution assay showing dose-dependent vancomycin suppression by pentamidine against wild type *E. coli* grown at 15°C. Dark regions represent higher cell density. **d,** Same as in **c**, except cells were transformed with the pGDP2 plasmid containing *mcr-1*. **e,** Atomic force microscopy of wild type *E. coli* grown at 37°C to mid-log phase (OD~0.5) in the presence of 25 μg/ml pentamidine. The white box (left) highlights the region scanned to obtain high-resolution topographical images of the cell surface (right).

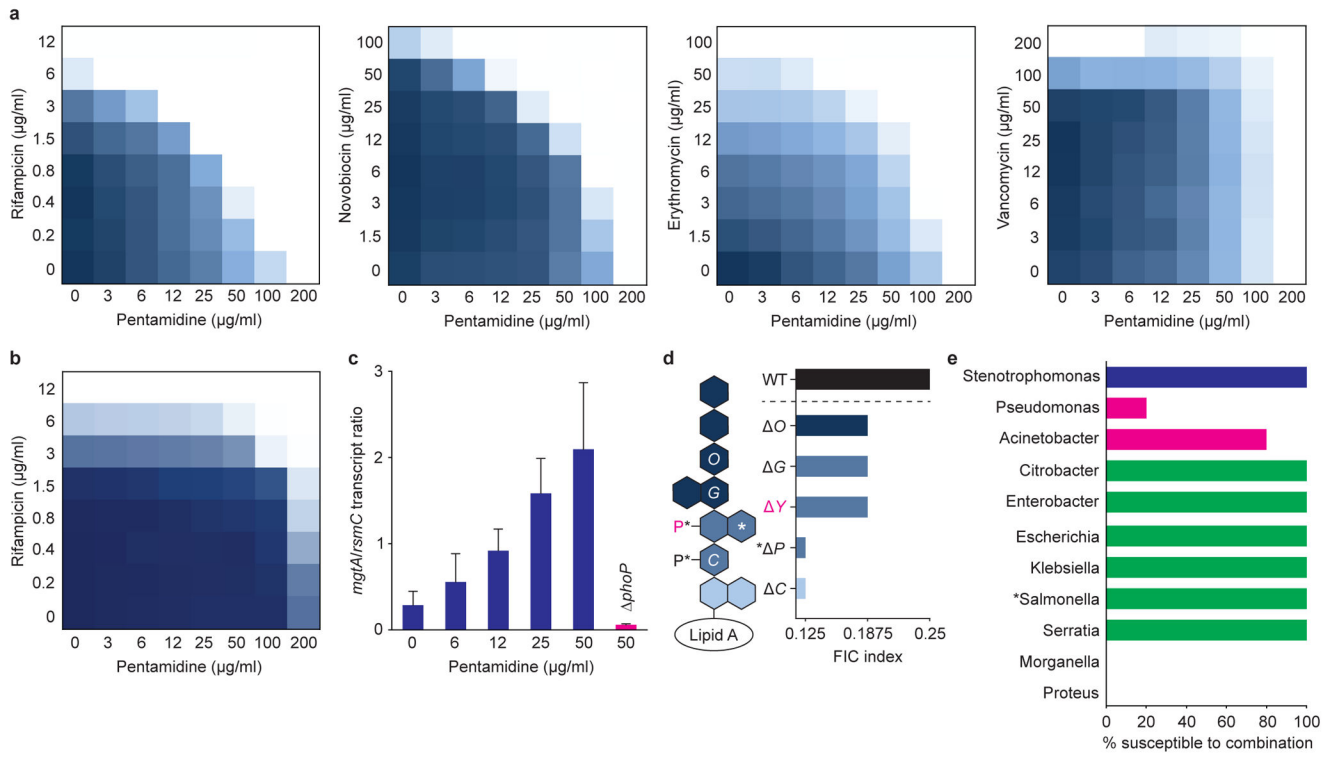

Figure 2. Pentamidine potentiates Gram-positive antibiotics in Gram-negative pathogens

a, Checkerboard broth microdilution assays between pentamidine and rifampicin, novobiocin, erythromycin, or vancomycin in wild type *E. coli* at 37°C. Dark regions represent higher cell density. **b,** Purified *E. coli* LPS (2 mg/ml) was added to growth medium, and wild type *E. coli* was grown in the presence of varying concentrations of pentamidine and rifampicin at 37°C. Dark regions represent higher cell density. **c,** Dose-dependent activation of the PhoPQ two-component system by pentamidine. Wild type *E. coli* (blue) and *E. coli* Δ*phoP* (pink) were grown at 37°C to mid-log phase (OD~0.5), and transcript levels of the PhoPQ-dependent gene *mgtA*[42] were quantified relative to the housekeeping gene *rsmC* using quantitative reverse transcription PCR. Data are the means with standard error from two biological replicates. **d,** Pentamidine-dependent potentiation of rifampicin against *E. coli* displaying various truncations in core OS. Cells were grown at 37°C and FIC indices were calculated using checkerboard broth microdilution assays as described in Methods. White letters indicate the Waa core OS biosynthetic gene that is responsible for addition of the corresponding residue. WaaY (pink) is necessary for the addition of phosphate to heptose II (pink). Loss of WaaP (*) prevents the addition of both core OS phosphates (*), as well as side-chain heptose III (*). Dark blue represents outer core OS; mid blue represents inner core OS; light blue represents 3-deoxy-D-*manno*-oct-2-ulosonic acid residues. **e,** Pentamidine-dependent potentiation of rifampicin against a spectrum of antibiotic resistant Gram-negative clinical isolates using checkerboard broth microdilution assays. The FIC index cutoff defining synergy was set to ≤0.5. Blue shows members of the Xanthomonadales; pink shows members of the Pseudomonadales; green shows members of the Enterobacteriales. At least 4 non-clonal isolates from each genus

were tested with the exception of *Salmonella* (*), for which only 1 clinical isolate was obtained.

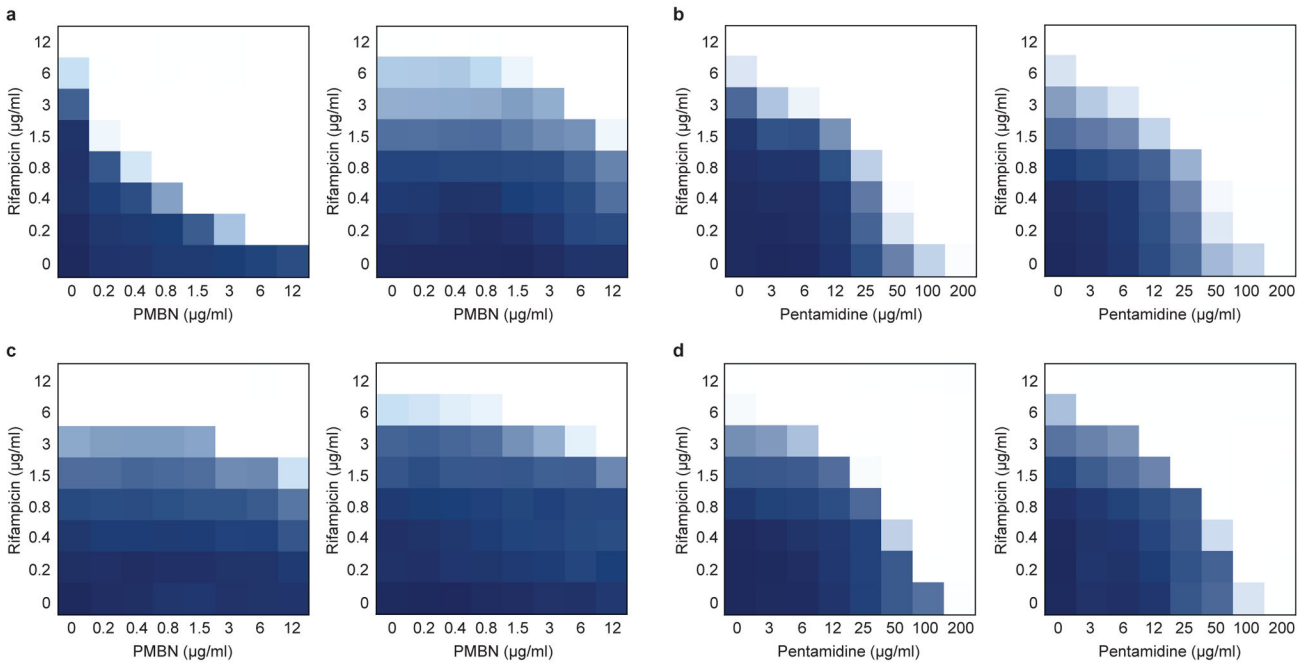

Figure 3. Pentamidine is an effective adjuvant against Gram-negative bacteria expressing *mcr-1*

a, Checkerboard broth microdilution assays showing dose-dependent rifampicin potentiation by PMBN against wild type *E. coli* (left) and *E. coli* expressing the *mcr-1* gene from the pGDP2 plasmid (right). The FIC index increases from ≤0.09 to ≤0.5 in the presence of *mcr-1*. **b,** Checkerboard broth microdilution assays showing dose-dependent rifampicin potentiation by pentamidine against wild type *E. coli* (left) and *E. coli* expressing the *mcr-1* gene from the pGDP2 plasmid (right). The FIC index is 0.25 irrespective of the presence of *mcr-1*. **c,** PMBN-dependent potentiation of rifampicin against two environmental isolates of *mcr-1* positive *E. coli*, N15-02865 (left) and N15-02866 (right), both of which were isolated from contaminated meat samples. **d,** Pentamidine-dependent potentiation of rifampicin against *mcr-1* positive *E. coli* strains N15-02865 (left) and N15-02866 (right). All experiments were performed at 37°C. Dark regions represent higher cell density.

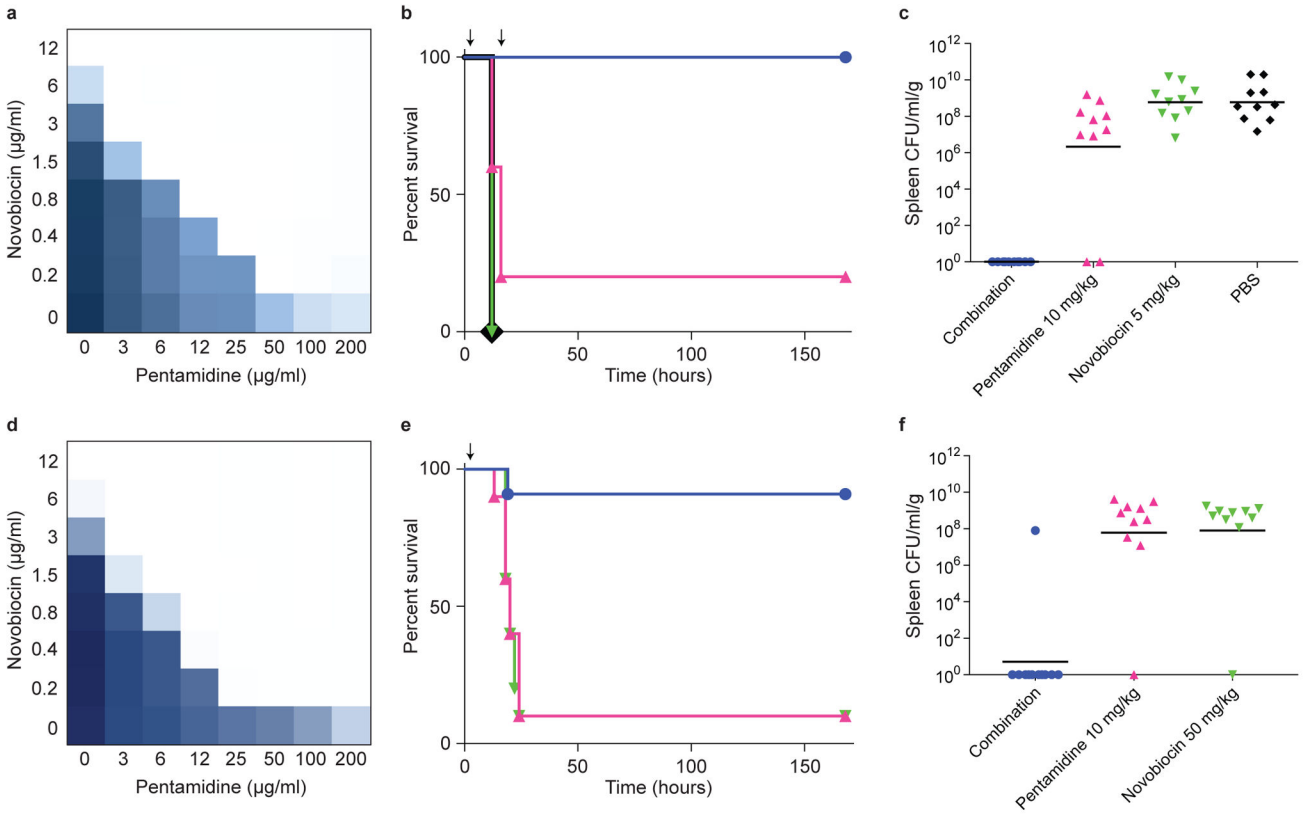

Figure 4. Pentamidine potentiates Gram-positive antibiotics against colistin-sensitive and -resistant *A. baumannii* in systemic murine infection models

a, Checkerboard broth microdilution assay showing dose-dependent novobiocin potentiation by pentamidine against colistin sensitive *A. baumannii* ATCC 17978 grown at 37°C. Dark regions represent higher cell density. **b,** Pentamidine-dependent potentiation of novobiocin in a systemic colistin sensitive *A. baumannii* ATCC 17978 murine infection model. ~2×10^6 CFU was injected intraperitoneally, and treatments were administered at 2-hours and 16-hours post-infection (arrows). Treatment groups (n=10) included PBS vehicle (black), 10 mg/kg pentamidine (pink), 5 mg/kg novobiocin (green), or a combination of 10 mg/kg pentamidine and 5 mg/kg novobiocin (blue). Phenotypic endpoint was defined using a body condition score as described in Methods. Experimental endpoint was defined as 7-days post-infection. **c,** Bacterial load in the spleen was determined by selective plating on chloramphenicol. Black lines represent geometric mean of the bacterial load for each treatment group. **d,** Checkerboard broth microdilution assay showing dose-dependent novobiocin potentiation by pentamidine against the colistin resistant variant of *A. baumannii* ATCC 17978. Cells were grown at 37°C. Dark regions represent higher cell density. **e,** Pentamidine-dependent potentiation of novobiocin in a systemic colistin resistant *A. baumannii* ATCC 17978 murine infection model. ~2×10^6 CFU was injected intraperitoneally, and a single treatment was administered at 2-hours post-infection (arrow). Treatment groups included 10 mg/kg pentamidine (pink; n=10), 50 mg/kg novobiocin (green; n=10), or a combination of 10 mg/kg pentamidine and 50 mg/kg novobiocin (blue; n=11). Phenotypic endpoint was defined using a body condition score as described in

Methods. Experimental endpoint was defined as 7-days post-infection. **f,** Bacterial load in the spleen was determined by selective plating on chloramphenicol. Black lines represent geometric mean of the bacterial load for each treatment group.

Table 1

Activity of pentamidine analogs against *E. coli*.

Analog	Structure	MIC_A	FIC_A	MIC_R	FIC_R	FIC Index
Pentamidine	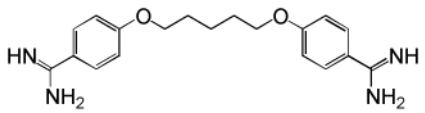	200	0.125	12	0.125	0.25
1	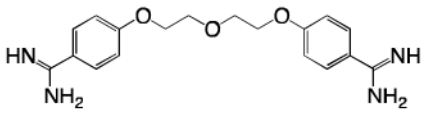	>200	<0.5	12	0.5	<1
2	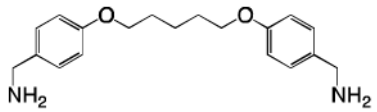	>200	<0.5	12	0.125	<0.625
3	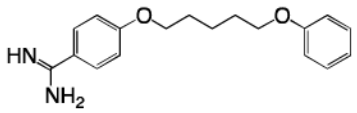	100	0.5	12	0.017	0.517
4	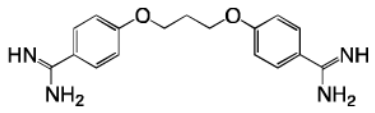	200	0.125	12	0.25	0.375
5	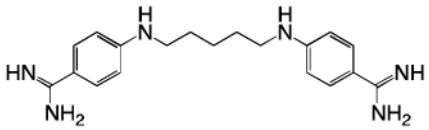	>200	<0.25	12	0.125	<0.375
6	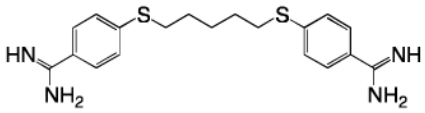	50	0.12	12	0.067	0.187

Analog	Structure	MIC_A	FIC_A	MIC_R	FIC_R	FIC Index
7	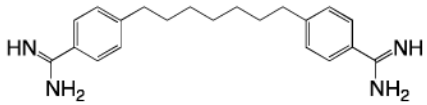	100	0.06	12	0.067	0.127
8	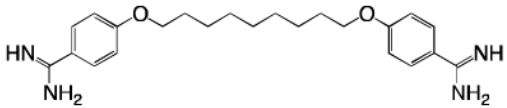	25	0.06	12	0.017	0.077
9	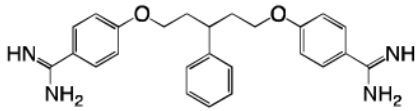	>200	<0.03	12	0.017	<0.047

Fractional inhibitory concentration (FIC) indices were calculated against *E. coli* using checkerboard broth microdilution assays with maximum concentrations of analog and rifampicin set to 200 μg/ml and 12 μg/ml, respectively. MIC_A is the minimum inhibitory concentration (MIC) of each analog alone; MIC_R is the MIC of rifampicin alone; FIC_A is the FIC of each analog; FIC_R is the FIC of rifampicin. FICx = [x]/MICx, where [x] is the lowest inhibitory concentration of drug in the presence of co-drug, and MICx is the MIC of x in the absence of co-drug; see Methods.